 doi:10.20944/preprints202209.0041.v1

Article

G-Net Light: A Lightweight Modified Google Net for Retinal Vessel Segmentation

Shahzaib Iqbal [1], Syed S. Naqvi [1], Haroon A. Khan [1], Ahsan Saadat[2], and Tariq M. Khan [3,*]

[1] Department of Electrical and Computer Engineering, COMSATS University Islamabad (CUI), Islamabad, Pakistan
[2] School of Electrical Engineering and Computer Science, National University of Sciences and Technology (NUST), Islamabad, Pakistan
[2] School of Computer Science and Engineering, University of New South Wales, Sydney, NSW, Australia
* Correspondence: tariq045@gmail.com

Abstract: Convolutional neural network architectures have become increasingly complex, which has improved the performance slowly on well-known benchmark datasets in the recent years. In this research, we have analyzed the true need for such complexity. We have introduced G-Net light, a lightweight modified GoogleNet with improved filter count per layer to reduce feature overlaps and complexity. Additionally, by limiting the amount of pooling layers in the proposed architecture, we have exploited the skip connections to minimize the spatial information loss. The investigations on the proposed architecture are evaluated on three retinal vessel segmentation publicly available datasets. The proposed G-Net light outperforms other vessel segmentation architectures by reducing the number of trainable parameters..

Keywords: Deep Learning; Convolutional Neural Networks; Medical Image Segmentation.

1. Introduction

Diabetic retinopathy has gained a great deal of attention recently due to its connection with long-standing diabetes that is one of the most common causes of avoidable blindness in the world [1]. Additionally, diabetic retinopathy is the major contributors of vision loss, especially in those of working age. Lesions are the first signs of DR, and they include exudates, microaneurysms, haemorrhages, vessel abnormalities and leakages [2,3]. As a result, the number and type of lesions that form on the surface of the retina affect the severity and diagnosis of the disease. As a result, the effectiveness of an automated system for extensive screening is anticipated to depend on the precision of segmenting blood vessels, optical cup/disc, and retinal lesions [4], [5]. Along these lines, it has long been thought that detecting retinal blood vessels is the most difficult problem, and it is frequently thought that it is the most crucial part of an automated computer-aided diagnostic (CAD) system [1], [6]. This is because the vessels in the retina are hard to see because of their tortuous shape, density, diameter, branching, and branching pattern. Even more challenging to identify are the centerline reflex and the many components that make up the retina, including the macula, optic cup/disc, exudates, and so on, all of which may have lesions or other flaws. Finally, the settings used for camera calibration and the acquisition method can also bring unpredictability into the imaging process. For the purpose of blood vessels segmentation, a machine/deep learning architecture is usually trained using a dataset of manually labelled segmented images [7]. In order to diagnose serious disorders including retinal vascular occlusions [8], glaucoma [9], AMD [10], DR [11], and chronic systematic hypoxemia (CSH) [12], these techniques have been used to detect retinal vessels. Furthermore, deep learning-based approaches have attained cutting-edge accuracy in applications including vessel detection and optic cup/disc detection [13]. Therefore, it is believed that the predominant technique for creating retinal diagnostics systems is now supervised machine learning models [14,15]. Despite considerable success of supervised ML models, it is still challenging to find blood vessels when there are noticeable contrast differences and abnormalities. It gets significantly more challenging when the vessels' diameter is small. Morever, training these architectures can takes a lot of time, despite the fact that the results of supervised segmentation obtained by these

 doi:10.20944/preprints202209.0041.v1

methods are superior to those of unsupervised segmentation. The lack of comprehensively (labelled) data for a variety of ailments and imaging modalities makes this more challenging. According to [16,17], the usage of intricate CNN architecture based models does not produce the optimal results for the majority of segmentation algorithms. Keep in mind that the quantity of hidden layers and the number of filters used in each layer have a significant impact on the number of trainable parameters. In these circumstances, shallow networks are frequently suggested as a deep network substitute [15]. In comparison to their deep counterparts, these shallow networks employ fewer filters per layer. Our network's layout is intended to utilize the most filters possible in each layer while minimizing the complexity of the system as a whole. If a picture has less feature variation, performance does not rise with more filters in a convolution layer, but complexity does. By recommending small-scale networks with few layers, convolution networks' complexity has been lowered in the literature [18,19]. Furthermore, the significance in terms of the performance and complexity is not addressed in [18]. Here, the characteristic complexity is used to determine the number of filters.

To the best of our knowledge, google Net based encoder decoder architecture for image segmentation is not proposed so far, so one of the major contribution of the proposed work is to design a decoder of GoogleNet. Inspired from the GoogleNet [20], this study introduces G-Net lite, a simple yet effective small scale neural network architecture for retinal blood vessels segmentation. This is because G-Net light only has a small number of parameters, which means that it requires relatively lesser memory and GPU resources than alternatives with significantly higher parameters. In addition, the encoder employs only two max-pooling layers to reduce the spatial information loss. Experiments are conducted on three different datasets of retinal blood vessels segmentation to demonstrate the efficacy of the proposed architecture for medical image segmentation.

2. G-Net Light

This section presents and explains the the proposed network architecture. In Fig. 1 overall architecture of G-Net light is presented. The proposed network starts with an input image layer, then a convolutional layer, and finally the essential final layers that create the pixel-wise segmentation map. We have performed non-linear activations (ReLU) on these segmentation map. The feature maps are then fed into the max-pooling layer. The inception block is used after the max-pooling layer, followed by another max-pooling layer. There is an inception block which connects the encoder and decoder blocks. At the decoder side, the up-sampling layer (max-unpooling) is used followed by the same inception block, another up-sampling layer and another inception block. Once the spatial information is restored using up-sampling layers, a convolutional layer (CL) followed by non-linear activations (ReLU), and the batch normalization layer (BN) is applied. After a soft-max layer, the final classification layer is a dice pixel classification layer. Note that the proposed architecture has four inception blocks, where the first block is used after the first down-sampling. There is an intermediary inception block that connects the encoder and decoder blocks. There are two inception blocks at decoder followed by the convolutional layer, which is supplied with the necessary final layers required for constructing the pixel-wise segmentation map. Using the convolution layers in between the filter banks and input feature maps, each encoder block creates its own collection of features. We have performed non-linear activations (ReLU) on these features. Depending on whether the block is up-sampling or down-sampling, the produced feature maps are subsequently supplied to the max-pooling or unpooling layers. All max-pooling and unpooling layers are 2×2, non-overlapping, with stride size of 2.

It is worth noting that the proposed network design responds to multiple motivations. To begin, we wanted to use as few pooling layers as possible in the proposed architecture. This is due to the fact that pooling frequently reduce the size of the feature maps and can also result in a spatial information loss. Second, we have used a limited number of convolutional layers. Finally, within each layer the total number of convolutional filters are minimized. Skip connections have been used between the encoder and the associated decoder blocks to preserve structural information. Figure 1 depicts these as doted lines with arrowheads. Another motivating force behind the choice to adopt skip connections as an alternative to dense skip paths is the assumption that feature retention within each convolutional layers may assist to reduce the semantic gap of the encoder side and decoder side while keeping computational overhead under control. In order to preserve fine-grained structures,

Preprints (www.preprints.org) | NOT PEER-REVIEWED | Posted: 5 September 2022 doi:10.20944/preprints202209.0041.v1

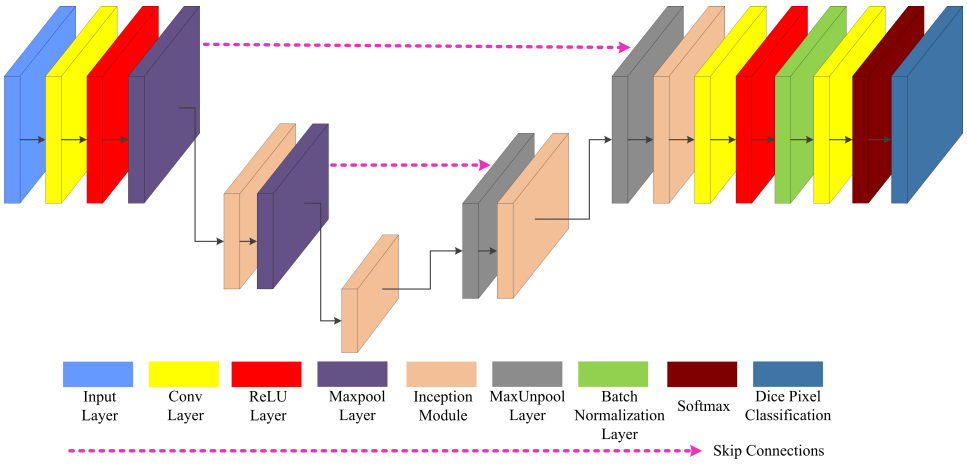

Figure 1. Block diagram of the proposed Network

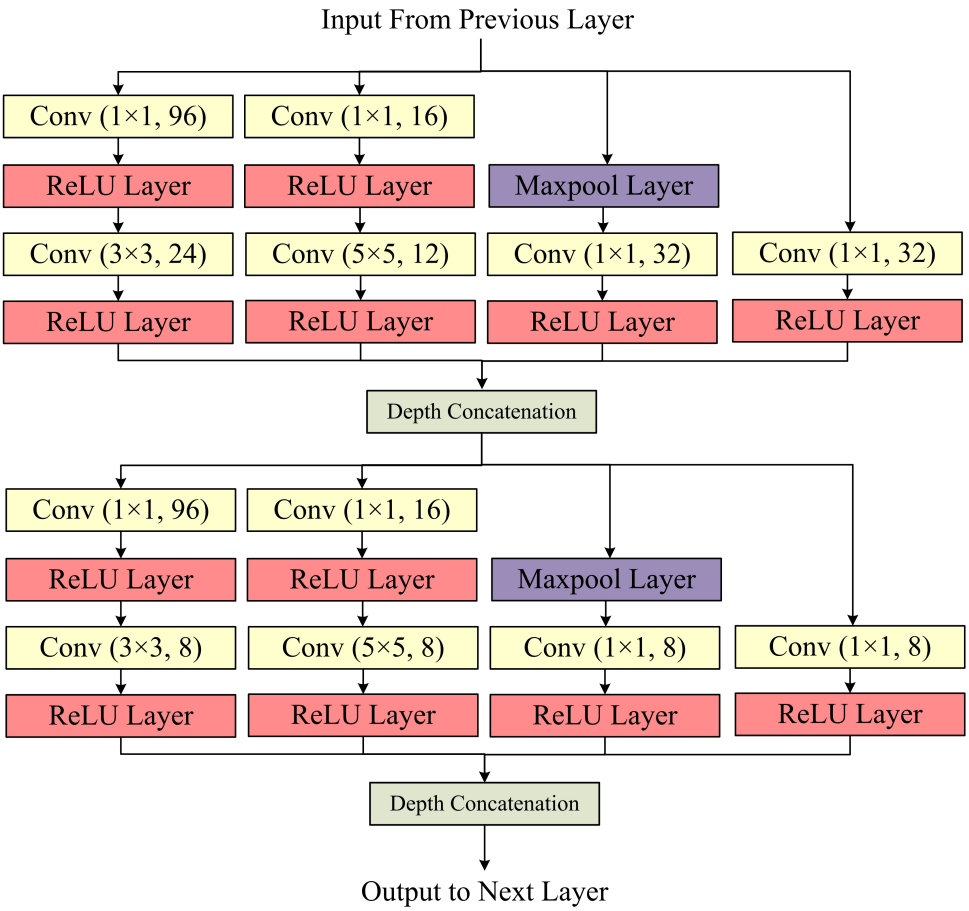

Figure 2. The Inception Block.

 doi:10.20944/preprints202209.0041.v1

which are frequently important in medical image segmentation, number of pooling layers are reduced in the proposed network.

2.1. The Inception Block

The key idea of the inception block is to apply the dimension reductions wisely.These reductions are computed using the 1×1 filter size for the convolutions operations prior to the 3×3 and 5×5 filter size for the convolutions operations. They are dual-purpose because, in addition to being utilised as reductions, they also utilise rectified linear activation. Fig. 2 depicts the ultimate design of the inception block. An Inception block generally is a architecture made up of the above-mentioned modules that are vertically stacked with intermittent max-pooling layers with stride 2, that result in the reduction of the grid's resolution. It appeared preferable to start using the inception blocks only at higher layers and leave the lower layers in typical convolutional form for technical reasons during the training. One of this architecture's key benefits is that it permits significant increases in the number of units at each step without increasing the complexity in terms of computations. The widespread use of reduction of the dimensions enables hiding the high volume of input filters from the preceding stage to the succeeding layer. This is achieved by initially lowering their dimension prior to convolving over them with a large patch size. This method also adheres to the idea that visual data should be processed at various scales before being aggregated, allowing the subsequent stage to simultaneously extract features from different scales. Because the processing resources are being used more efficiently, it is possible to increase both the total number of stages and the width of each stage without encountering computational challenges. Developing significantly less effective but computationally less expensive variations of the inception block is another way to use it. It can be seen that all of the available knobs and levers enable a controlled balancing of computational resources. This can lead to architectures that are twice as fast or three times as fast than similarly performing networks without the inception blocks, though this requires a careful manual design.

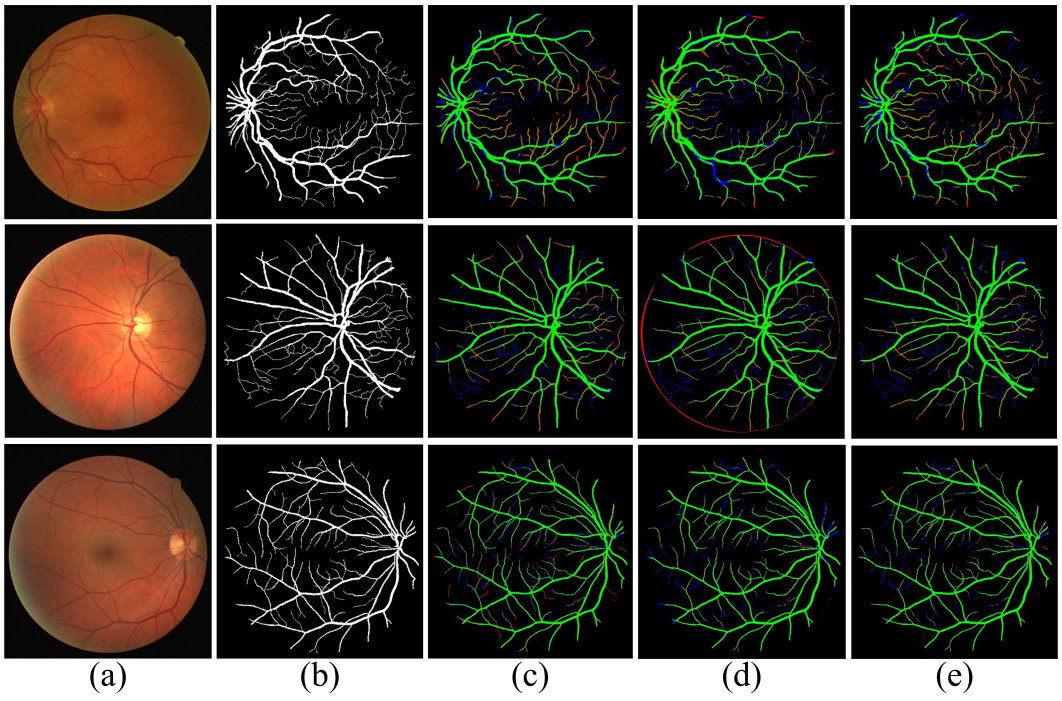

Figure 3. Analysis of Segmented Output. The segmentation maps' black and green colours represent accurately predicted pixels, whereas the blue and red colours represent false negatives and false positives, respectively.: (a) Noisy test image 3,4, and 19 of DRIVE dataset. (b) Ground truth images. (c) The output of SegNet [21]. (d) The output of U-Net [22]. (e) The output of the proposed G-Net light architecture.

Preprints (www.preprints.org) | NOT PEER-REVIEWED | Posted: 5 September 2022 doi:10.20944/preprints202209.0041.v1

3. Experimental Setup

3.1. Datasets

For the segmentation of retinal vessels, we tested our proposed network using three public image data sets: DRIVE [23], CHASE [24] and STARE [25]. DRIVE [23] was acquired from a DR screening program that took place in Netherlands. It is made up of 20 colour images for testing and 20 colour images for training, both of which are saved 584 × 565 image size in JPEG format and cover a wide range of age of DR patients. Minor signs of early mild DR are shown in seven images only. A field of view (FOV) binary mask is available for all images. Both the test and training images contain manually segmented ground truth vessels labels.

The CHASE [24] data set includes 28 colour images of 14 English schoolchildren. All images are acquired with a 30° FOV centred at the optical disc and an image resolution of 999×960 pixels. Two distinct manually segmentation ground truth maps are available. For the experiments, the first experts segmentation map is used. There are no defined training or testing sets in the CHASE dataset, so the training set consists of first 20 images, while the testing set consists the remaining 8 images.

The STARE [25] data set consists of 20 colour retinal fundus pictures with a size of 700 × 605 pixels per image that were taken at a 35° FOV. Ten of these twenty photos show pathologies. Each of these photos has two separate manual segmentation maps available. Here, we have used the initial ophthalmologist segmentation as the benchmark.

Table 1. Comparison results on the DRIVE dataset. Red is the best, green is the 2^{nd} best, and blue is the 3^{rd} best.

Method	Year	Sensitivity	Specificity	Accuracy	F1 - Score	Parameters(M)
SegNet[26]	2017	0.7949	0.9738	0.9579	0.8180	28.4
MS-NFN[27]	2018	0.7844	0.9819	0.9567	N.A	0.4
FCN[28]	2018	0.8039	0.9804	0.9576	N.A	0.2
BTS-DSN[29]	2019	0.7891	0.9804	-	N.A	7.8
Three-stage CNN[30]	2019	0.7631	0.9820	0.9538	N.A	N.A
DE U-Net[31]	2019	0.7986	0.9736	0.9511	N.A	N.A
EL Approach[32]	2019	0.7880	0.9819	0.9569	N.A	N.A
GGM[33]	2019	0.7820	0.9860	0.9600	N.A	N.A
VessNet[34]	2019	0.8022	0.9810	0.9655	N.A	9.0
Vessel-Net[35]	2019	0.8038	0.9802	0.9578	N.A	1.7
CcNet[36]	2020	0.7625	0.9809	0.9528	N.A	N.A
AWS FCM[37]	2022	0.7020	0.9844	0.9605	0.7531	N.A
Proposed Method	**2022**	**0.8192**	**0.9829**	**0.9686**	**0.8202**	**0.39**

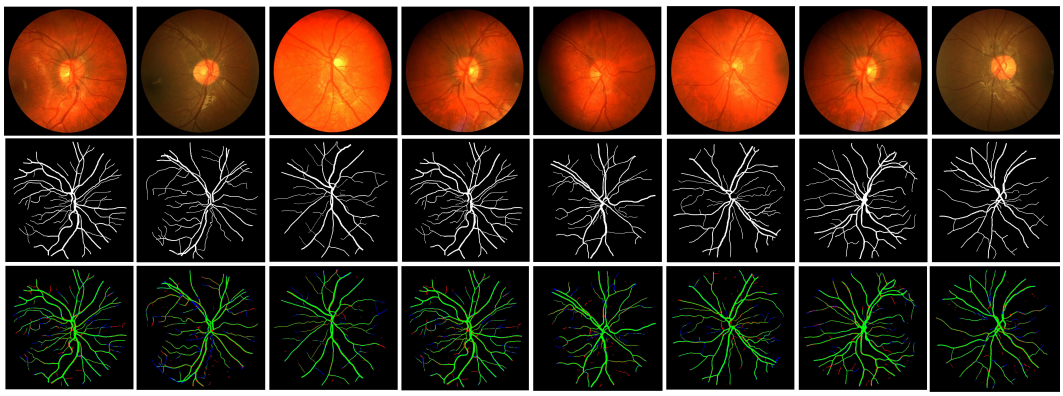

Figure 4. Analysis of Segmented Output. The segmentation maps' black and green colours represent accurately predicted pixels, whereas the blue and red colours represent false negatives and false positives, respectively.: In row one noisy test images of CHASE dataset. In row two corresponding ground truth images. In row three the output of the proposed network is presented.

Preprints (www.preprints.org) | NOT PEER-REVIEWED | Posted: 5 September 2022 doi:10.20944/preprints202209.0041.v1

3.2. Implementation and Training

All of our studies have been run using a GeForce GTX2080TI GPU and an Intel(R) Xeon(R) W-2133 3.6 GHz CPU with 96GB RAM. With a fixed learning rate, stochastic gradient descent was used in our RC-Net implementation. A weighted cross-entropy loss is employed as an objective function for training in all of our experiments. This decision was made after it was discovered that, in each retinal image's vessel segmentation, the "non-vessel" pixels outweighed the "vessel" pixels by a significant margin. Various techniques can be employed to assign the loss weights. Here, we use median frequency balancing to determine class association weights [26]. Keep in mind that there isn't a specific STARE test set accessible. In the literature, a "leave-one-out" strategy is frequently utilised for STARE [38]. With 10 photos for training and 10 for testing, we have employed both "leave-one-out" and precisely half-way data split in this case. We have also employed data augmentation to generate sufficient images for training since the retinal vascular segmentation image data sets used are relatively small. Contrast enhancement and rotations were utilised for the data augmentation. Each image is rotated by $1^o for the rotations at the training stage. The image brightness was randomly increased and decreased to enhan one - out trails.$

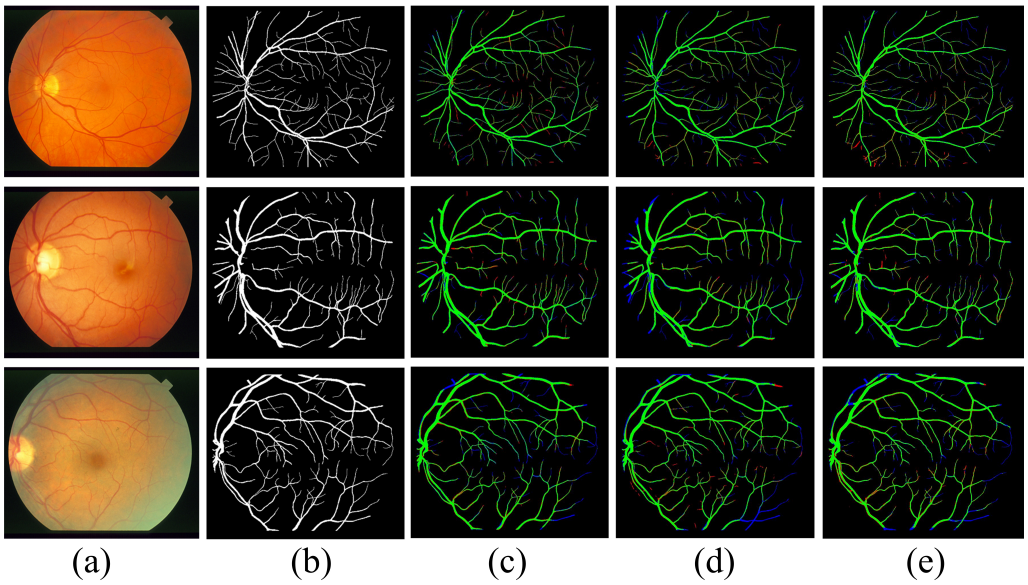

Figure 5. Analysis of Segmented Output. The segmentation maps' black and green colours represent accurately predicted pixels, whereas the blue and red colours represent false negatives and false positives, respectively.: (a) Noisy test images of STARE dataset. (b) Ground truth images. (c) The output of SegNet [21]. (d) The output of U-Net [22]. (e) The output of the proposed G-Net light architecture.

Table 2. Comparison results on the CHASE dataset. Red is the best, green is the 2^{nd} best, and blue is the 3^{rd} best.

Method	Year	Sensitivity	Specificity	Accuracy	F1 - Score
U-Net [39]	2016	0.7764	**0.9865**	0.9643	N.A
R2u-net [40]	2018	0.7756	0.9820	0.9634	N.A
Laddernet [41]	2018	0.7978	0.9818	0.9656	0.8031
Ce-net [42]	2019	0.8008	0.9723	0.9633	N.A
Iternet [43]	2020	0.7969	0.9820	0.9702	**0.8073**
SA-Unet [44]	2021	0.8151	0.9809	**0.9708**	0.7736
AACA-MLA-D-Unet [45]	2021	**0.8302**	0.9810	0.9673	**0.8248**
MC-UNet [46]	2022	**0.8366**	**0.9829**	**0.9714**	0.7741
Proposed Method	**2022**	**0.8210**	**0.9838**	**0.9726**	**0.8048**

Preprints (www.preprints.org) | NOT PEER-REVIEWED | Posted: 5 September 2022 doi:10.20944/preprints202209.0041.v1

3.3. Evaluation Criteria

Remember that pixel markings on blood vessels segmentation are binary, indicating whether a pixel is a vessel or the background. Publicly accessible datasets include *ground truth* that is manually annotated by experienced clinicians. As a result, each pixel is categorized as vessel pixel, if the area of interest is present in a image such as blood retinal vessels.There can be four possible outcomes for each output image: pixels that are correctly categorized as areas of interest (TP: true positive), pixels that are correctly categorized as non-interest (TN: true negative), pixels of non-interest that were incorrectly categorized (FP: false positive), and finally area of interest pixels that were falsely categorized as such ((FN): false negative). Four commonly used performance parameters Accuracy, Sensitivity, Specificity, and F1—score are frequently used in the literature to compare approaches using these components.

The term "Accuracy" in the equations above denotes the proportion of successfully segmented pixels to all of the pixels in the expertly annotated (labelled) mask. The *Sp* and *Se* indicate the model's specificity and sensitivity, which demonstrate how the no-vessel and vessel pixels are correctly distinguished. We also display the (AUC) for the receiver operating characteristic in the proposed vessel segmentation results (ROC). We did this because the distribution of positives and negatives in these data sets is imbalanced [47], and the $AUC - ROC$ is frequently regarded as a reliable indicator of how well a model can distinguish between negative classes and positive classes in the segmentation/classification problems.

4. Analysis of the Results and Comparisons

The qualitative and quantitative analysis of the proposed architecture with a number of commonly used alternatives methods in retinal image segmentation is done in this section. The qualitative segmentation findings for the retinal vessels on the DRIVE dataset are analyzed and discussed first. In the Fig. 3 the analysis of the segmented output is illustrated. In Fig. 3(a) noisy test image 3,4, and 19 from DRIVE dataset are presented. Corresponding ground truth images are given in Fig. 3(b). Fig. 3(c) - (d) presents the output of the networks SegNet [21] and U-Net [22], respectively. The segmentation output of the proposed architecture is given in Fig. 3(e). The segmentation maps' black and green colours represent accurately predicted pixels, whereas the blue and red colours represent false negatives and false positives, respectively. It is apparent that the suggested G-Net Light outperforms the U-Net [22] and SegNet [21] in terms of visual performance. The segmentation maps' black and green colours represent accurately predicted pixels, whereas the blue and red colours represent false negatives and false positives, respectively. It can be clearly observed that the visual performance of the proposed G-Net Light is better than the SegNet [21] and U-Net [22].

The vessel segmented maps of the proposed architecture on CHASE dataset are given in the Fig. 4. The segmentation maps' black and green colours represent accurately predicted pixels, whereas the blue and red colours represent false negatives and false positives, respectively. In the 1^{st} row noisy images of CHASE dataset are illustrated, and the corresponding ground truth images are shown in the 2^{nd} row of the Fig. 4. The final vessels segmented vessels map images of the proposed architecture are shown in the 3^{rd} row of the Fig. 4.

The Tables 1 - 2 compare the G-Net light network performance to some state-of-the-art supervised approaches. The proposed architecture obtains an average sensitivity of 81.92% for the DRIVE database and 82.10% for the CHASE database. In terms of the sensitivity parameter, the proposed G-Net light architecture outperforms all other techniques on DRIVE dataset, and is the 3^{rd} highest on CHASE dataset. The average accuracy of the proposed G-Net light is the 96.86% and 97.26% the highest on the DRIVE and CHASE datasets, respectively. The proposed architecture achieves an average specificity of 98.29% on DRIVE and 98.38% on CHASE the 3^{rd} and 2^{nd} highest respectively. Finally the proposed network achieves 82.02% of F1-score the highest on DRIVE dataset and the 3^{rd} highest value of 80.48% on CHASE dataset. It is worth mentioning that the each performance measure of the proposed network lies in top three values in comparison to other methods with only 0.39 millions trainable parameters only.

In the Fig. 5 the analysis of the segmented output is illustrated. In Fig. 5(a), Noisy test images from STARE dataset are presented. Corresponding ground truth images are given in Fig. 5(b). Fig. 5(c) - (d) presents the output of the networks SegNet [21] and U-Net [22], respectively. The

Preprints (www.preprints.org) | NOT PEER-REVIEWED | Posted: 5 September 2022 doi:10.20944/preprints202209.0041.v1

Table 3. Comparison results on the STARE dataset. Red is the best, green is the 2^{nd} best, and blue is the 3^{rd} best.

Method	Year	Sensitivity	Specificity	Accuracy	F1-Score
U-Net [39]	2016	0.7764	0.9865	0.9643	N.A
R2u-net [40]	2018	0.7756	0.9820	0.9634	N.A
Laddernet [41]	2018	0.7822	0.9804	0.9613	0.7994
BTS-DSN [29]	2019	0.8212	0.9843	N.A	N.A
Dual Encoding U-Net [31]	2019	0.7914	0.9722	0.9538	N.A
GGM [33]	2019	0.7960	0.9830	0.9610	N.A
Ce-net [42]	2019	0.7909	0.9721	0.9732	N.A
CcNet [36]	2020	0.7709	0.9848	0.9633	N.A
Iternet [43]	2020	0.7969	0.9823	0.9760	0.8073
SA-Unet [44]	2021	0.7120	0.9930	0.9521	0.7736
AACA-MLA-D-Unet [45]	2021	0.7914	0.9870	0.9665	0.8276
MC-UNet [46]	2022	0.7360	0.9947	0.9572	0.7865
Proposed Method	**2022**	**0.8170**	**0.9853**	**0.9730**	**0.8178**

vessels segmentation maps of the proposed architecture are shown in Fig. 5(e).The segmentation maps' black and green colours represent accurately predicted pixels, whereas the blue and red colours represent false negatives and false positives, respectively. It can be clearly observed that the visual performance of the proposed G-Net Light is better than the SegNet [21] and U-Net [22]. The Table 3 compare the proposed network performance to state-of-the-art supervised approaches. The proposed architecture obtains an average sensitivity of 81.70% ,which is 2^{nd} highest among the all methods. The average accuracy of the proposed G-Net light architecture is the 97.30%, which is 3^{rd} highest. Finally the proposed network achieves 81.78% of F1-score the 2^{nd} highest among the all methods on STARE dataset.

5. Conclusions

In this research paper, we have introduced and analyzed G-Net light, a lightweight modified GoogleNet with improved filter count per layer to reduce feature overlaps and complexity. Additionally, by reducing the amount of pooling layers in the proposed architecture, we have exploited the skip connections to minimize the spatial information loss. Our investigations are examined on publicly available DRIVE, CHASE, and STARE datasets. In the experiments, the proposed G-Net light outperforms other vessel segmentation architectures with fewer trainable number of parameters.

References

1. Khawaja, A.; Khan, T.M.; Naveed, K.; Naqvi, S.S.; Rehman, N.U.; Junaid Nawaz, S. An Improved Retinal Vessel Segmentation Framework Using Frangi Filter Coupled With the Probabilistic Patch Based Denoiser. *IEEE Access* **2019**, *7*, 164344–164361. https://doi.org/10.1109/ACCESS.2019.2953259.
2. Soomro, T.A.; Khan, T.M.; Khan, M.A.U.; Gao, J.; Paul, M.; Zheng, L. Impact of ICA-Based Image Enhancement Technique on Retinal Blood Vessels Segmentation. *IEEE Access* **2018**, *6*, 3524–3538.
3. Abdullah, F.; Imtiaz, R.; Madni, H.A.; Khan, H.A.; Khan, T.M.; Khan, M.A.U.; Naqvi, S.S. A Review on Glaucoma Disease Detection Using Computerized Techniques. *IEEE Access* **2021**, *9*, 37311–37333. https://doi.org/10.1109/ACCESS.2021.3061451.
4. Naveed, K.; Abdullah, F.; Madni, H.A.; Khan, M.A.; Khan, T.M.; Naqvi, S.S. Towards Automated Eye Diagnosis: An Improved Retinal Vessel Segmentation Framework Using Ensemble Block Matching 3D Filter. *Diagnostics* **2021**, *11*. https://doi.org/10.3390/diagnostics11010114.
5. Khan, M.A.; Khan, T.M.; Aziz, K.I.; Ahmad, S.S.; Mir, N.; Elbakush, E. The use of fourier phase symmetry for thin vessel detection in retinal fundus images. In Proceedings of the 2019 IEEE International Symposium on Signal Processing and Information Technology (ISSPIT). IEEE, 2019, pp. 1–6.
6. Imtiaz, R.; Khan, T.M.; Naqvi, S.S.; Arsalan, M.; Nawaz, S.J. Screening of Glaucoma disease from retinal vessel images using semantic segmentation. *Computers & Electrical Engineering* **2021**, *91*, 107036.
7. Khan, T.M.; Robles-Kelly, A.; Naqvi, S.S. A Semantically Flexible Feature Fusion Network for Retinal Vessel Segmentation. In Proceedings of the Neural Information Processing; Yang, H.; Pasupa, K.;

Leung, A.C.S.; Kwok, J.T.; Chan, J.H.; King, I., Eds.; Springer International Publishing: Cham, 2020; pp. 159–167.

8. Muraoka, Y.; Tsujikawa, A.; Murakami, T.; Ogino, K.; Kumagai, K.; Miyamoto, K.; Uji, A.; Yoshimura, N. Morphologic and Functional Changes in Retinal Vessels Associated with Branch Retinal Vein Occlusion. *Ophthalmology* **2013**, *120*, 91 – 99.
9. Thakoor, K.A.; Li, X.; Tsamis, E.; Sajda, P.; Hood, D.C. Enhancing the Accuracy of Glaucoma Detection from OCT Probability Maps using Convolutional Neural Networks. In Proceedings of the 2019 41st Annual International Conference of the IEEE Engineering in Medicine and Biology Society (EMBC), 2019, pp. 2036–2040.
10. Cicinelli, M.V.; Rabiolo, A.; Sacconi, R.; Carnevali, A.; Querques, L.; Bandello, F.; Querques, G. Optical coherence tomography angiography in dry age-related macular degeneration. *Survey of Ophthalmology* **2018**, *63*, 236 – 244. https://doi.org/https://doi.org/10.1016/j.survophthal.2017.06.005.
11. Zeng, X.; Chen, H.; Luo, Y.; Ye, W. Automated Diabetic Retinopathy Detection Based on Binocular Siamese-Like Convolutional Neural Network. *IEEE Access* **2019**, *7*, 30744–30753.
12. Traustason, S.; Jensen, A.S.; Arvidsson, H.S.; Munch, I.C.; Søndergaard, L.; Larsen, M. Retinal Oxygen Saturation in Patients with Systemic Hypoxemia. *Investigative Ophthalmology & Visual Science* **2011**, *52*, 5064.
13. Jiang, Y.; Zhang, H.; Tan, N.; Chen, L. Automatic Retinal Blood Vessel Segmentation Based on Fully Convolutional Neural Networks. *Symmetry* **2019**, *11*, 1112. https://doi.org/10.3390/sym11091112.
14. Khan, T.M.; Naqvi, S.S.; Arsalan, M.; Khan, M.A.; Khan, H.A.; Haider, A. Exploiting residual edge information in deep fully convolutional neural networks for retinal vessel segmentation. In Proceedings of the 2020 International Joint Conference on Neural Networks (IJCNN). IEEE, 2020, pp. 1–8.
15. Khan, T.M.; Abdullah, F.; Naqvi, S.S.; Arsalan, M.; Khan, M.A. Shallow Vessel Segmentation Network for Automatic Retinal Vessel Segmentation. In Proceedings of the 2020 International Joint Conference on Neural Networks, 2020, pp. 1–7. https://doi.org/10.1109/IJCNN48605.2020.9207668.
16. Chen, W.; Liu, Y.; Kira, Z.; Wang, Y.; Huang, J. A Closer Look at Few-shot Classification. In Proceedings of the International Conference on Learning Representations, 2019.
17. Kevin, M.; Serge, B.; Ser-Nam, L. A Metric Learning Reality Check. In Proceedings of the European Conference on Computer Vision, 2020, [2003.08505].
18. Howard, A.; Sandler, M.; Chu, G.; Chen, L.C.; Chen, B.; Tan, M.; Wang, W.; Zhu, Y.; Pang, R.; Vasudevan, V.; et al. Searching for MobileNetV3. In Proceedings of the Proceedings of the IEEE/CVF International Conference on Computer Vision (ICCV), 2019.
19. Ma, N.; Zhang, X.; Zheng, H.T.; Sun, J. ShuffleNet V2: Practical Guidelines for Efficient CNN Architecture Design. In Proceedings of the Proceedings of the European Conference on Computer Vision (ECCV), 2018.
20. Szegedy, C.; Liu, W.; Jia, Y.; Sermanet, P.; Reed, S.; Anguelov, D.; Erhan, D.; Vanhoucke, V.; Rabinovich, A. Going deeper with convolutions. In Proceedings of the Proceedings of the IEEE conference on computer vision and pattern recognition, 2015, pp. 1–9.
21. Tariq M., K.; Musaed, A.; Khursheed, A.; Muhammad, A.; Syed S., N.; S. Junaid, N. Residual Connection Based Encoder Decoder Network (RCED-Net) For Retinal Vessel Segmentation. *IEEE Access* **2020**.
22. Song, G. DPN: Detail-Preserving Network with High Resolution Representation for Efficient Segmentation of Retinal Vessels, 2020, [arXiv:eess.IV/2009.12053].
23. Staal, J.; Abramoff, M.D.; Niemeijer, M.; Viergever, M.A.; van Ginneken, B. Ridge-based vessel segmentation in color images of the retina. *IEEE Transactions on Medical Imaging* **2004**, *23*, 501–509.
24. The Child Heart and Health Study in England (CHASE), Accessed on: Jun 14, 2020.
25. Hoover, A.D.; Kouznetsova, V.; Goldbaum, M. Locating blood vessels in retinal images by piecewise threshold probing of a matched filter response. *IEEE Transactions on Medical Imaging* **2000**, *19*, 203–210.
26. Badrinarayanan, V.; Kendall, A.; Cipolla, R. SegNet: A Deep Convolutional Encoder-Decoder Architecture for Image Segmentation. *IEEE Transactions on Pattern Analysis and Machine Intelligence* **2017**, *39*, 2481–2495.
27. Wu, Y.; Xia, Y.; Song, Y.; Zhang, Y.; Cai, W. Multiscale Network Followed Network Model for Retinal Vessel Segmentation. In Proceedings of the Medical Image Computing and Computer Assisted Intervention, 2018, pp. 119–126.
28. Oliveira, A.; Pereira, S.; Silva, C.A. Retinal vessel segmentation based on fully convolutional neural networks. *Expert Systems with Applications* **2018**, *112*, 229–242.
29. Song, G.; Kai, W.; Hong, K.; Yujun, Z.; Yingqi, G.; Tao, L. BTS-DSN: Deeply supervised neural network with short connections for retinal vessel segmentation. *International Journal of Medical Informatics* **2019**, *126*, 105 – 113.

30. Yan, Z.; Yang, X.; Cheng, K. A Three-Stage Deep Learning Model for Accurate Retinal Vessel Segmentation. *IEEE Journal of Biomedical and Health Informatics* **2019**, *23*, 1427–1436. https://doi.org/10.1109/JBHI.2018.2872813.
31. Wang, B.; Qiu, S.; He, H. Dual Encoding U-Net for Retinal Vessel Segmentation. In Proceedings of the Medical Image Computing and Computer Assisted Intervention, 2019, pp. 84–92.
32. Ribeiro, A.; Lopes, A.P.; Silva, C.A. Ensemble learning approaches for retinal vessel segmentation. In Proceedings of the Proc. of Portuguese Meeting on Bioengineering. IEEE, 2019, pp. 1–4.
33. Khan, M.A.; Khan, T.M.; Naqvi, S.S.; Aurangzeb Khan, M. GGM classifier with multi-scale line detectors for retinal vessel segmentation. *Signal, Image and Video Process.* **2019**, *13*, 1667–1675.
34. Muhammad, A.; Muhamamd, O.; Tahir, M.; Se Woon, C.; Kang Ryoung, P. Aiding the Diagnosis of Diabetic and Hypertensive Retinopathy Using Artificial Intelligence-Based Semantic Segmentation. *Journal of Clinical Medicine* **2019**, *8*. https://doi.org/10.3390/jcm8091446.
35. Wu, Y.; Xia, Y.; Song, Y.; Zhang, D.; Liu, D.; Zhang, C.; Cai, W. Vessel-Net: Retinal Vessel Segmentation Under Multi-path Supervision. In Proceedings of the Medical Image Computing and Computer Assisted Intervention, 2019, pp. 264–272.
36. Feng, S.; Zhuo, Z.; Pan, D.; Tian, Q. CcNet: A cross-connected convolutional network for segmenting retinal vessels using multi-scale features. *Neurocomputing* **2020**, *392*, 268–276.
37. Mahapatra, S.; Agrawal, S.; Mishro, P.K.; Pachori, R.B. A novel framework for retinal vessel segmentation using optimal improved frangi filter and adaptive weighted spatial FCM. *Computers in Biology and Medicine* **2022**, *147*, 105770.
38. Soares, J.V.B.; Leandro, J.J.G.; Cesar, R.M.; Jelinek, H.F.; Cree, M.J. Retinal vessel segmentation using the 2-D Gabor wavelet and supervised classification. *IEEE Transactions on Medical Imaging* **2006**, *25*, 1214–1222.
39. Ronneberger, O..and Fischer, P.; Brox, T. U-Net: Convolutional Networks for Biomedical Image Segmentation. In Proceedings of the Medical Image Computing and Computer-Assisted Intervention, 2015, pp. 234–241.
40. Alom, M.Z.; Hasan, M.; Yakopcic, C.; Taha, T.M.; Asari, V.K. Recurrent residual convolutional neural network based on U-net (R2U-net) for medical image segmentation. *arXiv preprint arXiv:1802.06955* **2018**.
41. Zhuang, J. LadderNet: Multi-path networks based on U-Net for medical image segmentation. *arXiv preprint arXiv:1810.07810* **2018**.
42. Gu, Z.; Cheng, J.; Fu, H.; Zhou, K.; Hao, H.; Zhao, Y.; Zhang, T.; Gao, S.; Liu, J. Ce-net: Context encoder network for 2d medical image segmentation. *IEEE transactions on medical imaging* **2019**, *38*, 2281–2292.
43. Li, L.; Verma, M.; Nakashima, Y.; Nagahara, H.; Kawasaki, R. Iternet: Retinal image segmentation utilizing structural redundancy in vessel networks. In Proceedings of the Proc. of the IEEE/CVF Winter Conf. on Appl. of Comp. Vision, 2020, pp. 3656–3665.
44. Zhang, Q.L.; Yang, Y.B. Sa-net: Shuffle attention for deep convolutional neural networks. In Proceedings of the ICASSP 2021-2021 IEEE International Conference on Acoustics, Speech and Signal Processing (ICASSP). IEEE, 2021, pp. 2235–2239.
45. Yuan, Y.; Zhang, L.; Wang, L.; Huang, H. Multi-level attention network for retinal vessel segmentation. *IEEE Journal of Biomedical and Health Informatics* **2021**, *26*, 312–323.
46. Zhang, T.; Li, J.; Zhao, Y.; Chen, N.; Zhou, H.; Xu, H.; Guan, Z.; Yang, C.; Xue, L.; Chen, R.; et al. MC-UNet Multi-module Concatenation based on U-shape Network for Retinal Blood Vessels Segmentation. *arXiv preprint arXiv:2204.03213* **2022**.
47. Li, Q.; Feng, B.; Xie, L.; Liang, P.; Zhang, H.; Wang, T. A Cross-Modality Learning Approach for Vessel Segmentation in Retinal Images. *IEEE Transactions on Medical Imaging* **2016**, *35*, 109–118.